Not all spacetime coordinates for general-relativistic ray tracing are created equal

Gabriele Bozzola[*]

Department of Astronomy, University of Arizona, Tucson, Arizona, USA

Chi-kwan Chan[†]

Department of Astronomy, University of Arizona, Tucson, Arizona, USA;
Data Science Institute, University of Arizona, Tucson, Arizona, USA;
and Program in Applied Mathematics, University of Arizona, Tucson, Arizona, USA

Vasileios Paschalidis[‡]

Department of Astronomy, University of Arizona, Tucson, Arizona, USA
and Department of Physics, University of Arizona, Tucson, Arizona, USA

Models for the observational appearance of astrophysical black holes rely critically on accurate general-relativistic ray tracing and radiation transport to compute the intensity measured by a distant observer. In this paper, we illustrate how the choice of coordinates and initial conditions affect this process. In particular, we show that propagating rays from the camera to the source leads to different solutions if the spatial part of the momentum of the photon points towards the horizon or away from it. In doing this, we also show that coordinates that are well suited for numerical general-relativistic magnetohydrodynamic (GRMHD) simulations are typically not optimal for generic ray tracing. We discuss the implications for black hole images and show that radiation transport in optimal and nonoptimal spacetime coordinates lead to the same images up to numerical errors and algorithmic choices.

I. INTRODUCTION

The successful observations at the scale of black hole horizons by the Event Horizon Telescope (EHT) Collaboration [1–14] highlight the need for accurate general-relativistic ray tracing and radiation transfer. Ray tracing consists of finding the path that photons take from the hot plasma around black holes to our camera. In general relativity, we assume that these photons do not backreact onto the spacetime and are not quantum in nature, so the problem is equivalent to finding null geodesics (hereafter, rays).[1] Once the path of a ray is known, one has to perform radiation transfer. This consists of computing specific intensity and optical depth along the ray, assuming some

models for how they change due to the local thermodynamical properties of the plasma.[2] Ray tracing and radiation transfer are critical for the calibration, modeling, and interpretation of EHT results (e.g. [5,13,17,18]). They are also employed in accurate modeling of electromagnetic radiation from other compact objects such as stellar mass black holes [e.g., [19]] and neutron stars [e.g., [20,21]].

In this paper, we highlight how ray tracing is affected by choices of coordinate systems, initial conditions, and direction of integration (we will make this and other similar statements more precise below). First, we show that ray tracing is generally not invariant with respect to as time reversal: choosing our initial condition at the camera, integrating a geodesic between the source and the camera leads to two different results if the integration is performed forward (with the photon spatial momentum pointing towards the source) or backward in time (with the photon spatial momentum pointing away from the source). This is yet another example of how black holes defy our intuition.

---

[*]gabrielebozzola@arizona.edu
[†]chanc@arizona.edu
[‡]vpaschal@arizona.edu

[1]Understanding the geodesic structure is one of the primary tools in investigating spacetimes. Hence, the literature on the topic of general relativistic ray tracing is massive and spans several decades. At this point, there is a large number of codes available for ray tracing, several of which are public (for a noncomprehensive list see, e.g. [15]).

[2]A different approach, e.g., Monte Carlo radiative transfer [16], might be preferred if the system under consideration is dominated by scattering.

In nonrelativistic ray tracing (e.g., for computer graphics, or astronomy), there exist only one curve that connects a pixel of the camera to the source, and this curve can be found by shooting rays from the camera to the source. On this curve, information can freely flow in both the directions. This is no longer true in general relativity (unless both spacetime and the matter are also invariant with respect to time reversal).

Second, we discuss how some coordinate systems are better suited for ray tracing than others. In particular, coordinates used in stationary spacetime general-relativistic magnetohydrodynamic (GRMHD) simulations are typically not an optimal choice for ray tracing. The reason for this is that coordinates for GRMHD simulations are designed to let information flow towards the horizon, but ray tracing amounts to collecting information *from* the horizon, which is the opposite problem. Choice of non-optimal coordinates leads to numerical problems, and while gauge-invariant procedures ought to yield gauge-invariant results, in general this is not the case due to numerical considerations. We will show an explicit example in which the numerical error diverges due to the impossibility for numerical algorithms to properly resolve the geodesic. On the other hand, other coordinates lead to well behaved geodesics that numerical schemes can easily integrate. We will also discuss that in general the error in computing black hole images through general-relativistic radiation transfer is small.

The structure of the paper is as follows. In Sec. II, we review the fundamental tools that we need for the rest of the study: ray tracing and the Kerr-Schild (KS) coordinates. In Sec. III, we describe our findings focusing on the non-spinning case. This case is insightful as it can be more easily visualized and understood in terms of conformal diagrams.[3] Next, in Sec. IV we discuss the rotating case and the implications for black hole images. Finally, we collect our conclusions in Sec. V. We use units with $G = c = 1$, where G is the gravitational constant, and c the speed of light in vacuum. We use the same conventions as [22]: the signature of the metric is $(-, +, +, +)$, indices go from 0 to 3 (with 0 being the time component) and employ the Einstein summation convention for repeated indices.

II. SETUP

A. Ray tracing

General-relativistic ray tracing requires the solution of the geodesic equation for photons that reach an observer far away from the source. Let $x^\mu(\lambda)$ be the null geodesic we want to reconstruct, we have that

$$\frac{\mathrm{d}^2 x^\mu}{\mathrm{d}\lambda^2} = -\Gamma^\mu_{\alpha\beta} \frac{\mathrm{d}x^\alpha}{\mathrm{d}\lambda} \frac{\mathrm{d}x^\beta}{\mathrm{d}\lambda}, \tag{1}$$

where $\Gamma^\mu_{\alpha\beta}$ are the Christoffel symbols and λ is the affine parameter. We say that a geodesic $x^\mu(\lambda)$ is affinely parametrized when it satisfies Eq. (1). Christoffel symbols are symmetric in the lower indices and can be computed from the metric $g_{\alpha\beta}$ as

$$\Gamma^\mu_{\alpha\beta} = \frac{1}{2} g^{\mu\gamma}(\partial_\alpha g_{\beta\gamma} + \partial_\beta g_{\gamma\alpha} - \partial_\gamma g_{\alpha\beta}.). \tag{2}$$

This second order equation can be cast into a system of first order ones,

$$\frac{\mathrm{d}x^\mu}{\mathrm{d}\lambda} = k^\mu, \tag{3a}$$

$$\frac{\mathrm{d}k^\mu}{\mathrm{d}\lambda} = -\Gamma^\mu_{\alpha\beta} k^\alpha k^\beta. \tag{3b}$$

k^μ is the vector tangent to the geodesic, and it is a null vector, so it has to be that $k^\mu k_\mu = 0$ along the null geodesic. We will refer to this as the constraint of the problem.

Equations (3a) have to be supplemented with initial conditions for x^μ and k^μ. For this, we follow [23,24] in setting up a Cartesian grid with coordinates α and β (the pixels of our camera) perpendicular to the line of sight at a large Euclidean distance d from the source and inclination from the pole i and azimuthal angle j. As commonly done in the field, the inclination i is such that $i = 90°$ corresponds to the equatorial plane. For a given pixel, we choose the spatial components of k^μ such that they are perpendicular to the image plane and use the condition that $k^\mu k_\mu = 0$ to normalize k^t to 1. Setting $k^t = 1$ means that we can interpret the affine parameter λ as the coordinate time at the camera, and that time flows forward for increasing values of λ. With this choice, we will say that we integrate forward (backward) in time when we integrate with increasing (decreasing) values of λ. We will also say that the photon points towards (away from) the source if the spatial part of k^μ is outgoing from (ingoing to) the camera. In some codes, all these quantities are associated to integrals of motion (energy, angular momentum, and Carter constant).

We implement this scheme in a new code, kRay [25], where we solve Eq. (3a) numerically with the LSODA solver [26] of ODEPACK [27] through the SciPy interface [28]. The LSODA solver is accurate and robust, it has adaptive stepping and automatic stiffness detection (so that an implicit scheme is used when necessary), and can provide high-order interpolating functions. All the numerical integrations presented in this paper are performed setting 10^{-14} as absolute and relative tolerance, and all the calculations are in double precision.

---

[3]We would like to thank Erik Wessel for suggesting this way of looking at the problem.

B. Kerr-Schild coordinates

The Kerr spacetime describes a black hole with mass M and angular momentum Ma. In Cartesian Kerr-Schild (KS) coordinates (t, x, y, z), this is defined by the metric,

$$g_{\alpha\beta} = \eta_{\alpha\beta} + f l_\alpha l_\beta, \tag{4}$$

with $\eta_{\alpha\beta}$ being the flat-spacetime Minkowski metric in Cartesian coordinates, and

$$f = \frac{2Mr^3}{r^4 + a^2 z^2}, \tag{5}$$

$$l_\alpha = \left(\pm 1, \frac{rx + ay}{r^2 + a^2}, \frac{ry - az}{r^2 + a^2}, \frac{z}{r} \right), \tag{6}$$

where the plus and minus signs in the time component correspond to the *ingoing* and *outgoing* Kerr-Schild coordinates, respectively, and r is implicitly defined by

$$r^2 + a^2 \left(1 - \frac{z^2}{r^2} \right) = x^2 + y^2 + z^2. \tag{7}$$

In Cartesian Kerr-Schild, the horizon is a coordinate ellipsoid described by the equation,

$$\frac{x^2}{R_H^2 + a^2} + \frac{y^2}{R_H^2 + a^2} + \frac{z^2}{R_H^2} = 1, \tag{8}$$

with $R_H = M + \sqrt{M^2 - a^2}$. These coordinates are well defined everywhere (except at $r = 0$), they are horizon-penetrating, meaning that all the important fields (metric, Christoffel symbols, *et cetera*) are well-behaved on the horizon. For this reason, ingoing Kerr-Schild (or slight variations of them) are ubiquitously employed in numerical simulations of accretion flows [see, e.g., [29]]. We will use Kerr-Schild coordinates to discuss our findings but the issues presented are general features of general-relativistic ray tracing. Other coordinates that are commonly used are Boyer-Lindquist, which are not horizon penetrating for either ingoing or outgoing causal curves. Many of the early ray tracing codes (e.g., [20,30–35]) use the Boyer-Lindquist coordinates to take advantage of the symmetry of the spacetime and to reduce the computation cost.[4] However, supporting arbitrary coordinate systems (e.g., [16]) or adopting Kerr-Schild-like coordinates (e.g., [37]) is preferred for interacting with GRMHD simulations. Note that even if the geodesics of Kerr spacetimes are integrable and closed forms exist (e.g. [33,38]), as photon positions and momenta ($\propto k^\mu$) are frequently needed to sample the plasma along geodesics, in practice, it is often simpler and

faster to perform the integration numerically, which is what most codes do.

III. DIFFERENT COORDINATES LEAD TO DIFFERENT RESULTS

In this section, we identify and discuss two features of the ray-tracing scheme previously described. First, ray tracing leads to different results if the integration is performed forward in time with photon pointing towards the source or backward with photon pointing away (as defined in Sec. II A). Second, the choice of coordinates and initial conditions dictate which geodesics can be properly reconstructed, so some coordinate systems are better suited for ray tracing than others. We will present these results by considering a Kerr black hole with $a = 0$ (the Schwarzschild spacetime) in ingoing Kerr-Schild coordinates. In this case, we can understand most of the features we want to present using accessible equations and diagrams.

The problems we want to discuss already arise in one of the simplest cases: ray tracing a photon on the x axis (because of rotational symmetry, this is equivalent to any purely radial integrations). Let us focus on the $y = z = 0$ line with $x > 0$ (where $r = x$), we have that

$$ds^2 = -\left(1 - \frac{2M}{x}\right)dt^2 + \frac{4M}{x}dtdx + \left(1 + \frac{2M}{x}\right)dx^2, \tag{9}$$

where $ds^2 = g_{\mu\nu}dx^\mu dx^\nu$ is the element of proper spacetime length. We can understand most of the geodesic properties by looking at the null cones on this line. This is done by setting $ds^2 = 0$, defining $\dot{x} = dx/dt$,

$$\left(1 + \frac{2M}{x}\right)\dot{x}^2 + \frac{4M}{x}\dot{x} - \left(1 - \frac{2M}{x}\right) = 0. \tag{10}$$

Solving this, we find that

$$\frac{dx}{dt} = \frac{-\frac{2M}{x} \pm \sqrt{(\frac{2M}{x})^2 + (1 - \frac{2M}{x})(1 + \frac{2M}{x})}}{1 + \frac{2M}{x}}, \tag{11}$$

simplify,

$$\frac{dx}{dt} = -1 \quad \text{or} \quad \frac{dx}{dt} = \frac{x - 2M}{x + 2M}, \tag{12}$$

which, after integration, lead to

$$t(x) = -x + C_1 \quad \text{and} \quad t(x) = x + 4M\ln(x - 2M) + C_2, \tag{13}$$

with C_1, C_2 integration constants with units of M.

Equation (13) describes the null radial geodesics and establishes the existence of two families of solutions,

---

[4]See [36] for a discussion and comparison with the Boyer-Lindquist coordinates.
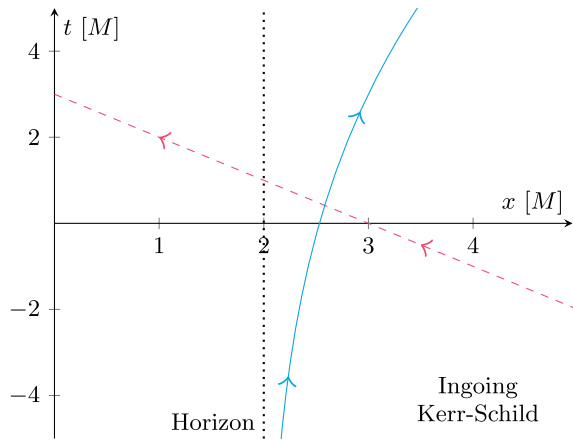
FIG. 1. Example of null geodesics in ingoing Kerr-Schild coordinates. Ingoing geodesics (arrows pointing towards $x = 0$) are horizon-penetrating and well-behaved. Outgoing (arrows pointing towards $x = +\infty$) geodesics are singular at the horizon. The choice of the direction of integration (forward or backward in time) determines which of the two families is being solved for. This shows that it is impossible for observers at infinity to collect information coming from inside the horizon.

ingoing $(dx/dt < 0)$ and outgoing photons $(dx/dt > 0)$. Figure 1 shows one example from each of these families on a spacetime diagram, where the ingoing ray is red dashed and the outgoing one is solid blue. Fixing $k^t = 1$ and assuming that integration starts from a camera far away (as in Sec. II A), the integration will select one of the two solutions depending on the initial conditions: when the geodesic is integrated forward in λ (i.e., with increasing values of λ) with the spatial part of k^μ pointing towards the source, the solution will be the ingoing one. The other one is selected when the geodesic is integrated backward in λ (i.e., with decreasing values of λ), with the spatial part of k^μ pointing away from the horizon (while still assuming $k^t = 1$). The existence of two distinct families demonstrates an important feature of general relativistic ray tracing: integrating photons backward in time is not the same as reversing their initial spatial momentum and integrating forward. Compare this with nonrelativistic ray tracing where one can shoot a ray and traverse it in both directions.[5]

Equation (13) shows that outgoing rays diverge exponentially at the finite radius $r = 2M$, while ingoing rays are always well behaved. For outgoing photons near the horizon, $\dot{x} \to 0$, which means that it takes an infinite amount of coordinate time t to make any infinitesimal step in x. In standard affine parametrizations, this manifests itself in $dt/d\lambda$ diverging near the horizon, as we explicitly show in the Appendix. Numerical schemes, even sophisticated
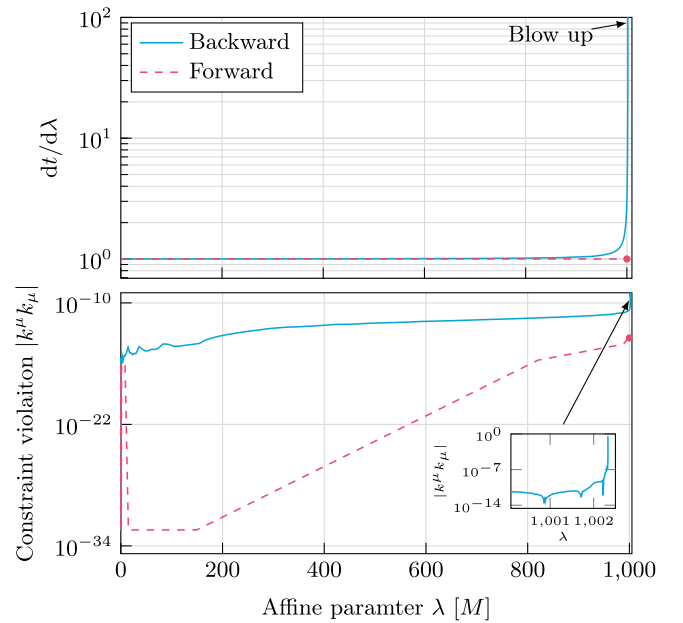

FIG. 2. Top: Time component of the photon four-velocity for a ray integrated backwards in time moving towards the camera and one integrated forward in time moving towards the horizon. (For the former, we redefined $\lambda \to -\lambda$ to enable the comparison). The filled circle indicates when the photon crosses the horizon. In the case of backward propagation, the photon never does so. The fast growth in $dt/d\lambda$ leads to a growth in the constraint violation as well, as shown in the bottom panel. Bottom: The constraint grows to arbitrary high values. The solution for the forward integration is constant, so the algorithm can take large steps (the entire solution took only 11 steps) and keep the error down. The filled circle indicates when the photon crosses the horizon. In the case of backward propagation, the photon never does so, and one has to impose some artificial prescription to end the integration.

ones, cannot accurately reconstruct this behavior. For instance, methods with adaptive time stepping will want to take an infinitesimally small step to keep the error under control. However, quickly the step becomes smaller than the finite precision of the machine and the integration cannot continue. This behavior is shown in Fig. 2, which depicts $dt/d\lambda$ on the top panel and the growth of the constraint (deviation of $|k^\mu k_\mu|$ from zero) in the second.

For outgoing rays, the photon will never touch the horizon in finite time given that $\dot{x} \to 0$.[6] Hence, the most natural termination condition for the numerical integration (the photon crossing the horizon) will never occur. As a result, one has to impose a different, artificial termination condition (e.g., stop the integration at some finite distance

---

[5]Assuming time-symmetric matter, integrating towards the horizon in ingoing coordinates is equivalent to integrating backwards in outgoing ones. This is not generally true for other spacetimes (including Kerr).

[6]Note, this is a general feature of event horizons, and it does not depend on the details of the coordinate chosen. Event horizon are defined as the boundary of causal past of future null infinity $\mathcal{I}^+$ [39], so no causal curve can connect events from inside the horizon to our camera. If the opposite were true, we would be able to see inside black holes.

from the horizon). Figure 2 shows that it is numerically impossible to reach distances that are arbitrarily close to the horizon, and the result of the integration will depend on a prescribed stopping condition. On the other hand, ingoing photons are perfectly well behaved and cross the horizon in finite time. In fact, the solution for ingoing photon is constant, so numerical schemes can capture this easily and accurately, and the entire solution requires a handful of steps to achieve an accuracy of better than 10^{-14}. In addition to keeping the error small, no artificial stopping condition has to be prescribed to terminate the integration. In other words, we can perfectly reconstruct the geodesics of ingoing photons, but we will always introduce errors in computing the ones for outgoing rays.

Figure 2 seems to suggest that ray tracing with integrated rays backward from the camera to the horizon is always bound to incur in significant numerical problems. We now show that this is purely a coordinate effect.[7] To do so, we move to *outgoing* Kerr-Schild coordinates by choosing the minus sign in Eq. (5). The transformation only changes the sign in front of the first $2M/x$ at the numerator of Eq. (11), so we the null cones satisfy

$$\frac{\mathrm{d}x}{\mathrm{d}t} = \frac{\frac{2M}{x} \pm 1}{\frac{2M}{x} + 1}. \qquad (14)$$

The two solutions are

$$\frac{\mathrm{d}x}{\mathrm{d}t} = 1 \qquad \frac{\mathrm{d}x}{\mathrm{d}t} = \frac{2M - x}{2M + x}. \qquad (15)$$

We can integrate these to obtain

$$t(x) = x + C_3 \quad t(x) = -x - 4M \ln(2M - x) + C_4, \qquad (16)$$

with C_3, C_4 integration constants with units of M. This change in coordinates completely flips the situation presented above. In the new coordinates, the outgoing null rays are well-behaved and the ingoing ones are not. For static spacetimes, we can perform an isometric identification to map the outgoing geodesic in the outgoing coordinates to the ingoing geodesic in the ingoing coordinates. Therefore, only in these spacetimes (which include Schwarzschild but not Kerr), it makes sense to integrate towards the source. Note that is no longer true in presence of nonstatic sources. In other words, for Schwarzschild, moving from ingoing Kerr-Schild to outgoing Kerr-Schild is equivalent to reversing the integration of the photon. So, we can read Fig. 2 as comparing the two coordinate systems for outgoing rays (with red dashed line showing the result in outgoing Kerr-Schild and the solid blue line in ingoing ones).

---

[7]Similar conclusions were obtained in [40]. Another example of the use of outgoing Kerr-Schild coordinates in the context of ray tracing is [41].

This simple case shows that if we want to perform accurate ray tracing integrating backward in time, the outgoing Kerr-Schild coordinates are a superior choice. This conclusion is ultimately a statement about the causal structure of the coordinates and does not depend on the specific example considered. Ingoing Kerr-Schild coordinates are a good choice for numerical simulations because matter can easily flow inside the horizon, but they are not suitable for ray tracing, where we want to propagate information from regions near the horizon. In Sec. III A, we discuss a possible way to implement stable integrations in ingoing Kerr-Schild.

Figure 3 shows the conformal diagram for maximally extended Schwarzschild spacetime. This plot, representing null geodesics as lines at 45° angle, concisely explains all the features that we have described so far. Our Universe is described by region I and our camera C is a timelike observer lying at a constant large radius. The boundary between region I and II is known as the future event horizon, and that between region I and IV (the past event horizon). The green solid line with light cones represents the world line of a parcel of plasma that will eventually fall into the horizon. Ray tracing and radiation transfer consists of modeling and collecting all the emission from these fluid elements.

First, we can see directly that integration backward and forward in time, as defined earlier, lead to different geodesics (compare the dashed black arrow line originating from the camera C with the orange solid line). So, when we perform ray tracing, we have to integrate backwards from the camera C with momentum pointing away from the horizon. Second, we can understand the relative performance between the two Kerr-Schild coordinates by looking at which quadrants they describe. Ingoing Kerr-Schild describes regions I and II, so that we can follow the trajectory of the fluid element towards the horizon. When we perform ray tracing along the orange geodesic, we run into a coordinate singularity near the boundary with region IV. The geodesic is not complete, and there is a coordinate barrier on that boundary, which is felt when $r \to 2M$. On the other hand, outgoing Kerr-Schild describes region I and IV, so we can reconstruct the geodesic in its entirety, and there are no issues with coordinates.

A. Mitigating numerical instabilities by integrating in coordinate time

In Sec. III, we discussed how it is not possible to achieve long-term stability in numerical integration of null geodesics in coordinate systems that are not well adapted to the problem. In the case of Kerr-Schild, the horizon is a coordinate singularity, and the impossibility of extending some geodesics past it is a pure gauge effect that manifests itself in the uncontrollable growth of k^t. A possible way to continue the integration without running in numerical problems is to perform the geodesic integration in
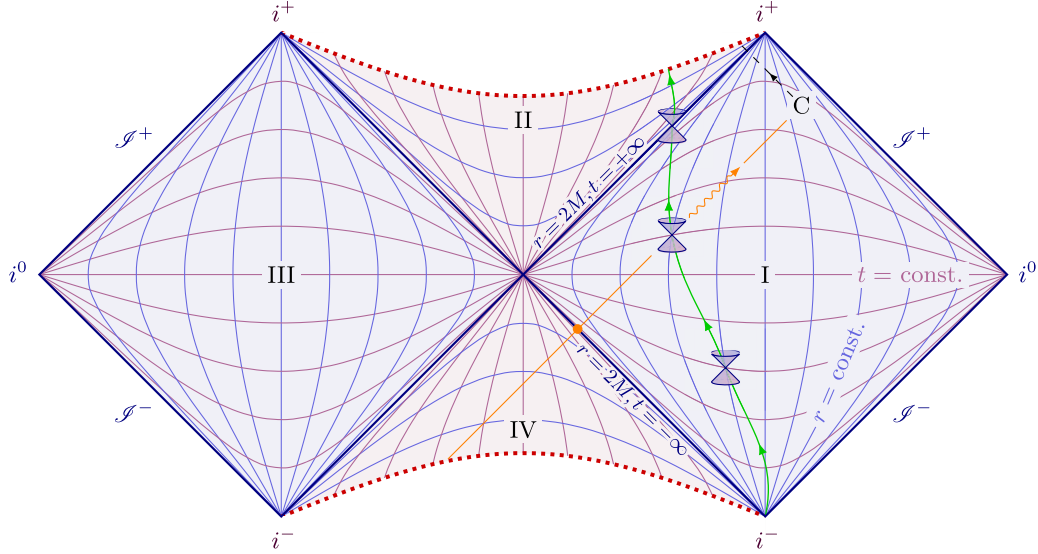
FIG. 3.   Conformal diagram for a maximally-extended Schwarzschild spacetime (the angular dimensions are suppressed). Null geodesics are inclined with a 45° angle, with future directed ones moving towards $\mathscr{I}^+$. The ingoing Kerr-Schild coordinates only cover regions I and II, the outgoing ones region I and IV. Our Universe is region I. Constant time and radius curves are hyperbolas (purple and blue respectively). We place our camera C at a large separation from the horizon and trace back the emission along the orange line. For the ingoing Kerr-Schild coordinates, the propagation hits a coordinate singularity at $r = 2M$ at the past horizon (orange dot) because that part of the spacetime is not mapped in these coordinates, whereas integration proceeds uninhibited until the physical singularity in the outgoing coordinates. The diagram also shows how integrating backward and forward in time results in two different geodesics: the orange one (backward) and the black dashed one (forward). The world line of the fluid element from which we collect emission is in green. Emission that is detectable from our cameras only comes from particles in region I. The problem with performing ray-tracing in ingoing coordinates is that there is "coordinate barrier" at $r = 2M$ at the past horizon, so numerical algorithms fail.

coordinate time t as opposed to affine parameter λ. To do so, the equation that has to be solved is

$$\frac{d^2 x^\mu}{dt^2} = \left(\Gamma^0_{\alpha\beta} \frac{dx^\mu}{dt} - \Gamma^\mu_{\alpha\beta} \right) \frac{dx^\alpha}{dt} \frac{dx^\beta}{dt}. \tag{17}$$
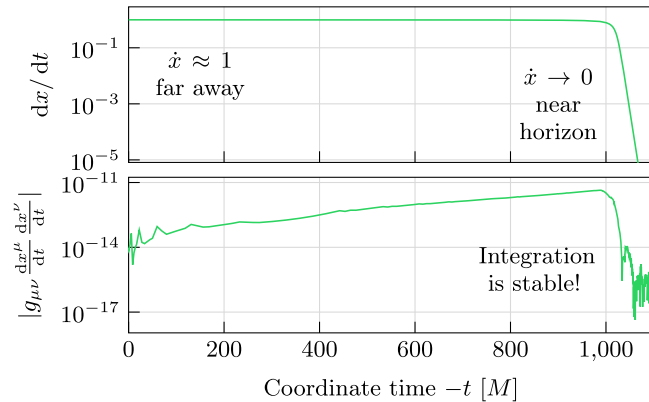
Figure 4 shows that the formulation is stable.

FIG. 4.   Backward propagation in coordinate time. This scheme does not have numerical problems, and the integration can be carried on for arbitrarily long times. The photon will take an infinite amount of time to reach the horizon. $\dot{x}$ drops to zero near unstable part of the integration is pushed to infinity.

Let us derive Eq. (17). Consider a geodesic described by $x^\mu(\lambda) = (t(\lambda), x^i(\lambda))$ with $i \in \{1, 2, 3\}$, and λ is the affine parameter. Starting from Eq. (1),

$$\frac{d^2 x^\mu}{d\lambda^2} = -\Gamma^\mu_{\alpha\beta} \frac{dx^\alpha}{d\lambda} \frac{dx^\beta}{d\lambda}, \tag{18}$$

we set $\mu = 0$ and find

$$\frac{d^2 t}{d\lambda^2} = -\Gamma^0_{\alpha\beta} \frac{dx^\alpha}{d\lambda} \frac{dx^\beta}{d\lambda}, \tag{19}$$

Using the chain rule, we have that

$$\frac{d^2 x^\mu}{d\lambda^2} = \frac{d}{d\lambda} \left(\frac{dx^\mu}{d\lambda} \right) = \frac{d}{d\lambda} \left(\frac{dx^\mu}{dt} \frac{dt}{d\lambda} \right). \tag{20}$$

According to the Leibniz rule and applying again the chain rule on the first term, we obtain

$$\frac{d}{d\lambda} \left(\frac{dx^\mu}{dt} \frac{dt}{d\lambda} \right) = \left(\frac{dt}{d\lambda} \right)^2 \frac{d^2 x^\mu}{dt^2} + \frac{d^2 t}{d\lambda^2} \frac{dx^\mu}{dt}. \tag{21}$$

Using Eq. (19), we can write

$$\left(\frac{\mathrm{d}t}{\mathrm{d}\lambda}\right)^2 \frac{\mathrm{d}^2 x^\mu}{\mathrm{d}t^2} + \frac{\mathrm{d}^2 t}{\mathrm{d}\lambda^2} \frac{\mathrm{d}x^\mu}{\mathrm{d}t} = \tag{22}$$

$$\left(\frac{\mathrm{d}t}{\mathrm{d}\lambda}\right)^2 \frac{\mathrm{d}^2 x^\mu}{\mathrm{d}t^2} - \Gamma^0_{\alpha\beta} \frac{\mathrm{d}x^\alpha}{\mathrm{d}\lambda} \frac{\mathrm{d}x^\beta}{\mathrm{d}\lambda} \frac{\mathrm{d}x^\mu}{\mathrm{d}t} = \tag{23}$$

$$\left(\frac{\mathrm{d}t}{\mathrm{d}\lambda}\right)^2 \frac{\mathrm{d}^2 x^\mu}{\mathrm{d}t^2} - \Gamma^0_{\alpha\beta} \left(\frac{\mathrm{d}t}{\mathrm{d}\lambda}\right)^2 \frac{\mathrm{d}x^\alpha}{\mathrm{d}t} \frac{\mathrm{d}x^\beta}{\mathrm{d}t} \frac{\mathrm{d}x^\mu}{\mathrm{d}t}, \tag{24}$$

where we applied the chain rule in the last step. The left-hand-side of Eq. (18) can be substituted with Eq. (24), using the chain rule on that equation one more time, eliminating $(\mathrm{d}t/\mathrm{d}\lambda)^2$ and rearranging terms, we find

$$\frac{\mathrm{d}^2 x^\mu}{\mathrm{d}t^2} = \left(\Gamma^0_{\alpha\beta} \frac{\mathrm{d}x^\mu}{\mathrm{d}t} - \Gamma^\mu_{\alpha\beta}\right) \frac{\mathrm{d}x^\alpha}{\mathrm{d}t} \frac{\mathrm{d}x^\beta}{\mathrm{d}t}. \tag{25}$$

Note that this equation is well-defined only when $\mathrm{d}t/\mathrm{d}\lambda$ is finite. Analytically, this condition is always satisfied except on the horizon.

The ultimate reason why this formulation works is because we traded an integration in a finite time (but that diverges), with one that takes an infinite amount of time and becomes unstable only for $t \to \infty$. With this formulation, we can integrate arbitrarily long in the past without running into numerical problems, as shown in Fig. 4, which reports the constraint violation for the same setup described in Sec. III. While this formulation works, calculations with analytical models will produce more accurate results if using improved coordinate systems described in the main text. In practice, with an appropriate coordinate transformation [36], this formulation is also useful for ray-tracing GRMHD simulations, which typically use ingoing Kerr-Schild and where a natural cutoff in coordinate time when to stop the integration already exists.

IV. BLACK HOLE IMAGES

The high degree of symmetry of the Schwarzschild spacetime allowed us to clearly analyze the problem and understand what happens in terms of equations and diagrams. This is no longer possible for most other spacetimes, including Kerr. Nonetheless, the features described in the previous section are presented in those cases as well, and when coordinates are not adapted to the problem it is not possible to fully integrate the geodesics. In this section, we look at the more general rotating case and highlight features that only depend on the coordinates used. Next, we discuss gauge-invariant observables, like black hole images and shadows.

Figure 5 shows the constraint violation ($|k^\mu k_\mu|$, where k^μ is $\mathrm{d}x^\mu/\mathrm{d}\lambda$) for a photon integrated in ingoing or outgoing Kerr-Schild coordinates. Note that the spinning case differs from the Schwarzschild one in the important fact that it is not symmetric with respect to time reversal. Therefore, the
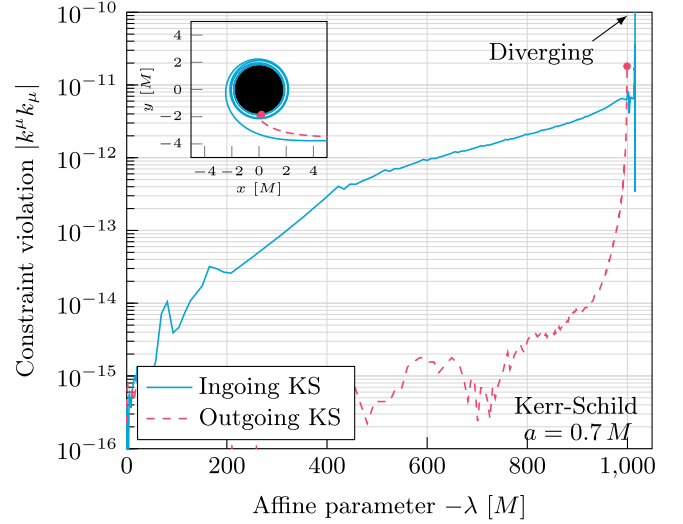

FIG. 5. Numerical violation of the null condition for a null geodesic with screen coordinates $\alpha = -3.559\,45M$, $\beta = 0$. The geodesic is integrated backwards in both the ingoing (solid blue line) and outgoing (red dashed line) Kerr-Schild coordinates with black hole spin $a = 0.7M$. Both integrations identify that the photon comes from the horizon, but one does so in a regular fashion (red dashed line), and the blue one takes an infinite amount of time (solid blue line). The filled circle indicates when the photon crosses the horizon. In the inset, we show the trajectories of the photons in their own evaluated coordinate systems.

geodesic obtained when integrating photons towards the source is not the correct one to use for radiation transfer. So, here we always integrate backwards in time with momentum pointing away from the horizon. The figure shows that the integration is well-behaved only for outgoing coordinates, in which case we can reconstruct the entirety of the geodesic without running into numerical problems. When we use ingoing Kerr-Schild coordinates, the constraint violation diverges. Photons that fall into the horizon in the ingoing metric spend an infinite amount of time orbiting the black hole in the outgoing ones. In doing this, they accumulate numerical error for the same reason highlighted in Sec. III. One possible remedy implemented by previous studies is to impose a boundary condition so that the integration is stopped at a distance that is larger than the distance at which the photon orbits, and an alternative approach is presented was Sec. III A (integrating with respect to the coordinate time). We find here the same conclusion we found in the previous section: using an optimal set of coordinates results in higher accuracy and significantly higher performance, as it was shown in the bottom panel of Fig. 2, where the entire solution was obtained with a handful of steps.

While some quantities depend critically on the gauge, the difference in performance between the two coordinate systems has marginal effects on coordinate-independent observables. Analytically, quantities that are obtained
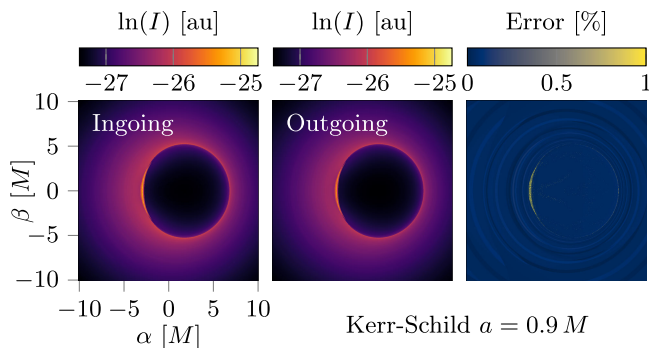
FIG. 6. Measured intensity from a stationary fluid configuration emitting with thermal bremsstrahlung on different coordinate systems. The camera is on the equatorial plane ($\iota = 90°$, $\jmath = 0°$) at a Euclidean distance d of $1 \times 10^3 M$. Intensity is measured in arbitrary units (au). Error (right panel) is computed as the relative difference between the two solutions generated integrating the rays backward in time in the ingoing (left panel) and outgoing (middle panel) Kerr-Schild coordinates.

through gauge-independent processes do not depend on the choice of coordinates, but this is not necessarily true numerically because of the numerical error and *ad hoc* fixes or termination conditions. The accumulated numerical error near the horizon can change results: Figs. 2 and 5 show that the violation of the constraint ($k^\mu k_\mu = 0$, the null condition for the geodesic) explodes, meaning that the integration becomes less and less accurate. In addition to that, arbitrary termination conditions truncate prematurely the geodesics. In practice, in the case of ill-suited coordinate systems, a ray will orbit the horizon an infinite amount of times but the contribution to the specific intensity is suppressed in the process.[8] Hence, the missing amount of the flux compared to case with coordinates that are better suited for ray tracing is minimal.

In Fig. 6, we compare the image produced by performing gauge-invariant radiation transport *backward in time* in both ingoing and outgoing Kerr-Schild coordinates with spin $a = 0.9$. The radiation transfer is implemented as in Eqs. (19) and (20) in [42]. For this image, we consider a toy example with a stationary fluid with four-velocity $(1/\sqrt{-g_{tt}}, 0, 0, 0)$ distributed with density that goes as $1/R$, where R is the Euclidean distance from the center of the black hole. The fluid has a fixed temperature, and we assume its emissivity is thermal bremsstrahlung [43]. This fluid configuration is not realistic but similar results are obtained with other setups. Figure 6 shows the resulting image and shows that the fractional difference is small. To reduce the difference between the two images one has to

move the integration termination criterion closer and closer to the real horizon, and move the final coordinate time to larger and larger values in the past. Due to the numerical errors described in Sec. III and Sec. IV, in practice, it is impossible to obtain perfect convergence with finite-precision codes.

A second quantity that is often studied in the literature is the black hole shadow (also known as the critical curve [17]). These computations of are also not much affected by the choice of coordinates because they rely on binary identification (whether the photon comes from the horizon). Even if integrations in ingoing coordinates collect significant errors and cannot be completed, most stopping criteria will correctly identify whether the photon originated from the horizon. For this reason, the computation will not be affected by the large errors.

In conclusion, if one has access to an analytical spacetime and fluid model, we recommend using coordinates that are adapted to the problem of ray tracing. In the other cases, gauge-invariant calculations will still produce robust results.

V. CONCLUSIONS

Ray tracing is a fundamental tool for our understanding of the observational appearance of black holes. In this paper, we discussed how general relativistic ray tracing is dependent on the adopted chart. In Sec. III, we showed that in general the process is not time reversible and integrating the geodesic equations towards the source forward and backward in time lead to different results. This is against our common intuition, according to which, there is only one light ray that connects our eyes to a given object. We also discussed properties of coordinates and showed that charts that are designed to facilitate the flow of information into horizons are not optimal choices for ray tracing. Using the best set of coordinates results in significantly higher accuracy and performance. Hence, we recommend to use suitable coordinates for those studies that use analytical spacetimes and matter configurations. As shown in Sec. III A, integrating in coordinate time is a good solution for other cases (e.g., in GRMHD simulations). In Sec. IV, we discussed how some quantities depend on the coordinates and showed that for gauge-independent observables (like black hole images obtained with radiation transfer) the numerical problems can lead to small errors.

---

[8]If I_ν is the specific intensity $dI_\nu/d\lambda \propto \nu^{-1}$, where ν is the redshift factor [42]. Unless one designed a pathological fluid configuration, ν diverges with k^t in ingoing Kerr-Schild coordinates, so the contribution to the specific intensity vanishes as the photon orbits the horizon.

APPENDIX: INTEGRATING THE RADIAL GEODESIC IN THE SCHWARZSCHILD SPACETIME

In Sec. III, we discussed the properties of the radial geodesics in Schwarzschild spacetimes by looking at the null cones. Here, we provide a full integration of the geodesic equation for outgoing solutions in affine parameter and in ingoing Kerr-Schild coordinates.

Equation (13) provides the relationship between x and t for null outgoing geodesics; let us compute $x(\lambda)$ and $t(\lambda)$, where λ is the affine parameter. Let us define $\kappa = d\lambda/dt$, from the geodesic equation (1), we have that (as long as κ is finite and nonzero)

$$\frac{d\kappa}{dt} = \kappa \Gamma^t_{\alpha\beta} \frac{dx^\alpha}{dt} \frac{dx^\beta}{dt}. \tag{A1}$$

The Christoffel symbols for metric (9) are

$$\Gamma^t_{tt} = \frac{2M^2}{x^3},$$
$$\Gamma^t_{tx} = \Gamma^t_{xt} = \frac{M(2M+x)}{x^3},$$
$$\Gamma^t_{xx} = \frac{2M(M+x)}{x^3}.$$

From Eq. (12), we have that $\dot{x} = (x - 2M)/(x + 2M)$, so we can find the differential equation,

$$\frac{1}{\kappa}\frac{d\kappa}{dx} = \frac{4M}{(x-2M)(x+2M)}. \tag{A2}$$

We can solve this equation with separation of variables,

$$\ln\kappa = \ln(x - 2M) - \ln(x + 2M) + K, \tag{A3}$$

with K constant of integration, which we can fix to zero by assuming that $\kappa = 1$ for $x \to +\infty$. Therefore, we have that

$$\kappa(x) = \frac{x - 2M}{x + 2M}. \tag{A4}$$

From Eq. (15), we recognize dx/dt on the left-hand-size of this last equation, which, coupled with the definition of κ, leads to

$$\frac{d\lambda}{dt} = \frac{dx}{dt}. \tag{A5}$$

Integration of this equation shows that x is an affine parameter. We conclude that

$$x(\lambda) = \lambda + L, \tag{A6}$$

where L is a constant that can be determined by demanding that $x(0)$ is the location of the camera. Plugging in Eq. (12), we find the expression for $t(\lambda)$.

[1] K. Akiyama, A. Alberdi, W. Alef, K. Asada, R. Azulay, A.-K. Baczko, D. Ball, M. Baloković, J. Barrett *et al.* (Event Horizon Telescope Collaboration), Astrophys. J. Lett. **875,** L1 (2019).

[2] K. Akiyama, A. Alberdi, W. Alef, K. Asada, R. Azulay, A.-K. Baczko, D. Ball, M. Baloković, J. Barrett *et al.* (Event Horizon Telescope Collaboration), Astrophys. J. Lett. **875,** L2 (2019).

[3] K. Akiyama, A. Alberdi, W. Alef, K. Asada, R. Azulay, A.-K. Baczko, D. Ball, M. Baloković, J. Barrett *et al.* (Event Horizon Telescope Collaboration), Astrophys. J. Lett. **875,** L3 (2019).

[4] K. Akiyama, A. Alberdi, W. Alef, K. Asada, R. Azulay, A.-K. Baczko, D. Ball, M. Baloković, J. Barrett *et al.*

(Event Horizon Telescope Collaboration), Astrophys. J. Lett. **875,** L4 (2019).

[5] K. Akiyama, A. Alberdi, W. Alef, K. Asada, R. Azulay, A.-K. Baczko, D. Ball, M. Baloković, J. Barrett *et al.* (Event Horizon Telescope Collaboration), Astrophys. J. Lett. **875,** L5 (2019).

[6] K. Akiyama, A. Alberdi, W. Alef, K. Asada, R. Azulay, A.-K. Baczko, D. Ball, M. Baloković, J. Barrett *et al.* (Event Horizon Telescope Collaboration), Astrophys. J. Lett. **875,** L6 (2019).

[7] K. Akiyama, J. C. Algaba, A. Alberdi, W. Alef, R. Anantua, K. Asada, R. Azulay, A.-K. Baczko, D. Ball *et al.* (Event Horizon Telescope Collaboration), Astrophys. J. Lett. **910,** L12 (2021).

[8] K. Akiyama, J. C. Algaba, A. Alberdi, W. Alef, R. Anantua, K. Asada, R. Azulay, A.-K. Baczko, D. Ball *et al.* (Event Horizon Telescope Collaboration), Astrophys. J. Lett. **910**, L13 (2021).

[9] K. Akiyama *et al.* (Event Horizon Telescope Collaboration), Astrophys. J. Lett. **930**, L12 (2022).

[10] K. Akiyama *et al.* (Event Horizon Telescope Collaboration), Astrophys. J. Lett. **930**, L13 (2022).

[11] K. Akiyama *et al.* (Event Horizon Telescope Collaboration), Astrophys. J. Lett. **930**, L14 (2022).

[12] K. Akiyama *et al.* (Event Horizon Telescope Collaboration), Astrophys. J. Lett. **930**, L15 (2022).

[13] K. Akiyama *et al.* (Event Horizon Telescope Collaboration), Astrophys. J. Lett. **930**, L16 (2022).

[14] K. Akiyama *et al.* (Event Horizon Telescope Collaboration), Astrophys. J. Lett. **930**, L17 (2022).

[15] R. Gold, A. E. Broderick, Z. Younsi, C. M. Fromm, C. F. Gammie, M. Mościbrodzka, H.-Y. Pu, T. Bronzwaer, J. Davelaar, J. Dexter *et al.*, Astrophys. J. **897**, 148 (2020).

[16] J. C. Dolence, C. F. Gammie, M. Mościbrodzka, and P. K. Leung, Astrophys. J. Suppl. Ser. **184**, 387 (2009).

[17] S. E. Gralla, D. E. Holz, and R. M. Wald, Phys. Rev. D **100**, 024018 (2019).

[18] Z. Younsi, D. Psaltis, and F. Özel, Astrophys. J. **942**, 47 (2023).

[19] J. D. Schnittman, J. H. Krolik, and S. C. Noble, Astrophys. J. **819**, 48 (2016).

[20] M. Bauböck, D. Psaltis, F. Özel, and T. Johannsen, Astrophys. J. **753**, 175 (2012).

[21] M. Bauböck, D. Psaltis, and F. Özel, Astrophys. J. **872**, 162 (2019).

[22] C. W. Misner, K. S. Thorne, and J. A. Wheeler, *General Relativity* (W.H. Freeman and Co., San Francisco, CA, 1973).

[23] D. Psaltis and T. Johannsen, Astrophys. J. **745**, 1 (2012).

[24] C.-k. Chan, D. Psaltis, and F. Özel, Astrophys. J. **777**, 13 (2013).

[25] G. Bozzola, C.-k. Chan, and V. Paschalidis, kRay: general-relativistic ray tracing and radiation transport in arbitrary spacetimes (to be published).

[26] L. Petzold, SIAM J. Sci. Stat. Comput. **4**, 136 (1983).

[27] A. Hindmarsh and L. L. Laboratory, *ODEPACK, a Systematized Collection of ODE Solvers* (Lawrence Livermore National Laboratory, Livermore, California, 1982).

[28] P. Virtanen, R. Gommers, T. E. Oliphant, M. Haberland, T. Reddy, D. Cournapeau, E. Burovski, P. Peterson, W. Weckesser, J. Bright *et al.*, Nat. Methods **17**, 261 (2020).

[29] C. F. Gammie, J. C. McKinney, and G. Tóth, Astrophys. J. **589**, 444 (2003).

[30] V. Karas, D. Vokrouhlicky, and A. G. Polnarev, Mon. Not. R. Astron. Soc. **259**, 569 (1992).

[31] S. U. Viergutz, Astron. Astrophys. **272**, 355 (1993), https://articles.adsabs.harvard.edu/pdf/1993A%26A...272..355V.

[32] K. P. Rauch and R. D. Blandford, Astrophys. J. **421**, 46 (1994).

[33] J. Dexter and E. Agol, Astrophys. J. **696**, 1616 (2009).

[34] D. Psaltis and T. Johannsen, Astrophys. J. **745**, 1 (2012).

[35] C.-k. Chan, D. Psaltis, and F. Özel, Astrophys. J. **777**, 13 (2013).

[36] P. Christian and C.-k. Chan, Astrophys. J. **909**, 67 (2021).

[37] C.-k. Chan, L. Medeiros, F. Özel, and D. Psaltis, Astrophys. J. **867**, 59 (2018).

[38] S. E. Gralla and A. Lupsasca, Phys. Rev. D **101**, 044032 (2020).

[39] R. M. Wald, *General Relativity* (Chicago University Press, Chicago, IL, 1984).

[40] P. Pihajoki, M. Mannerkoski, J. Nättilä, and P. H. Johansson, Astrophys. J. **863**, 8 (2018).

[41] A. Riazuelo, Int. J. Mod. Phys. D **29**, 2050109 (2020).

[42] Z. Younsi, K. Wu, and S. V. Fuerst, Astron. Astrophys. **545**, A13 (2012).

[43] G. B. Rybicki and A. P. Lightman, *Radiative Processes in Astrophysics* (John Wiley & Sons, Weinheim, Germany, 1986).

[44] D. Stanzione, J. West, R. T. Evans, T. Minyard, O. Ghattas, and D. K. Panda, in *Practice and Experience in Advanced Research Computing* (Association for Computing Machinery, New York, NY, USA, 2020), PEARC '20, pp. 106–111, ISBN: 9781450366892.

[45] O. Tange, GNU parallel (2021), GNU parallel is a general parallelizer to run multiple serial command line programs in parallel without changing them, 10.5281/zenodo.6377950.

[46] C. R. Harris, K. J. Millman, S. J. van der Walt, R. Gommers, P. Virtanen, D. Cournapeau, E. Wieser, J. Taylor, S. Berg, N. J. Smith *et al.*, Nature (London) **585**, 357 (2020).

[47] M. M. McKerns, L. Strand, T. Sullivan, A. Fang, and M. A. G. Aivazis, arXiv:1202.1056.

[48] A. Meurer, C. P. Smith, M. Paprocki, O. Čertík, S. B. Kirpichev, M. Rocklin, A. Kumar, S. Ivanov, J. K. Moore, S. Singh *et al.*, PeerJ Comput. Sci. **3**, e103 (2017).

[49] G. Bozzola, J. Open Source Softwaare **6**, 3099 (2021).